On-line Monitoring of Mechanical Faults in Variable-Speed Induction Motor Drives Using the Wigner Distribution

Martin Blödt, *Student Member, IEEE*, David Bonacci, Jérémi Regnier, Marie Chabert, and Jean Faucher

***Abstract*— This paper examines the detection of mechanical load faults in induction motors during speed transients by stator current analysis. Mechanical load faults generally lead to load torque oscillations at specific frequencies, related to the mechanical rotor speed. The torque oscillations produce a characteristic sinusoidal phase modulation of the stator current. Speed transients result in time-varying supply frequencies that prevent the classical, Fourier transform based spectral estimation. This paper proposes the use of a time-frequency distribution, the Wigner Distribution, for stator current analysis. Fault indicators are extracted from the distribution for on-line condition monitoring. The proposed methods are implemented on a DSP and experimental results in steady-state and during transients are presented.**

***Index Terms*— Fault detection, induction motor, mechanical fault, motor current signature analysis, torque oscillation, Wigner Distribution.**

I. Introduction

INDUCTION motors are used in a wide variety of industrial applications. In order to increase the productivity, reliability and safety of an installation containing induction motors, permanent and automatic motor condition monitoring is often desired.

Stator current based condition monitoring is often advantageous due to easy and economical implementation. The monitoring is in most cases done in steady operation state using classical spectral analysis tools. However, a lot of drives are adjustable speed drives where mechanical speed transients may be present during a long time period. The resulting time-varying supply frequency prevents the use of classical spectral analysis. The application of other signal processing methods like time-frequency analysis overcomes this problem and makes condition monitoring possible during speed transients.

This paper investigates the detection of torque oscillations caused by mechanical faults in induction machines using stator current time-frequency analysis. In a general way, a fault in the load part of the drive will be seen from the induction machine by a periodic variation of the load torque that is no longer constant. Examples for such faults causing torque oscillations include:

- general fault in the load part of the drive system e.g. load unbalance
- shaft misalignment
- gearbox faults e.g. broken tooth
- bearing faults

Torque oscillations already exist in a healthy motor due to space and time harmonics of the airgap field, but the considered fault related torque oscillations are present at particular frequencies, often related to the mechanical motor speed.

Thomson showed in [1] that mechanically induced speed oscillations give rise to sidebands of the fundamental stator current frequency f_s. It was also demonstrated that shaft misalignment causes a rise at frequencies $f_s \pm f_r$ in the current spectrum where f_r is the shaft rotational frequency. Obaid et. al. [2] studied load unbalance and shaft misalignment and proposed a detection scheme based on monitoring stator current frequencies at $f_s \pm f_r$. Kral et. al. [3] analyzed the instantaneous motor input power to detect mass imbalance and eccentricity. Nevertheless, the power measurement requires 3 voltage and 3 current transducers. All the cited works consider steady state motor operation at constant supply frequency. The employed FFT based spectral analysis methods cannot be used during speed and frequency transients. Several time-frequency methods are proposed in [4] for the detection of load torque oscillations in induction motors with time-varying supply frequencies. In [5], rotor faults in brushless DC motors are detected during transients using Wigner-Distributions. The algorithm has also been implemented on a DSP.

In this work, the induction motor stator current is analyzed during transients i.e. variable supply frequencies using Wigner Distributions. It is shown that small load torque oscillations lead to a particular signature on the distribution that is used to derive two different fault indicators. These methods are implemented on a low-cost DSP in order to demonstrate their computational effectiveness.

Section II resumes the effect of load torque oscillations on the stator current. The resulting fault model shows a sinusoidal phase modulation at the fault characteristic frequency. In section III, the chosen signal processing method i.e. the Wigner Distribution is presented and the theoretical fault signature is calculated. The following section IV deals with the DSP implementation of the proposed processing scheme, including the necessary filtering, downsampling, numerical calculation of the Wigner Distribution and the fault indicators. Section V describes the experimental setup used to generate small periodic torque oscillations at the rotational frequency. The theoretically predicted fault signature on the Wigner Distribution is validated. Experimentally obtained fault indicators

Corresponding author: Martin Blödt, email: martin.blodt@leei.enseeiht.fr
Address: Laboratoire d'Electrotechnique et d'Electronique Industrielle, 2 rue Camichel, 31071 Toulouse, France. Tel: +33 561 588084

are presented for different amplitudes of the torque oscillation corresponding to different fault levels under different load conditions and with varying supply frequencies. The Wigner Distribution based indicators are compared to the classical spectrum based approach in steady state in order to demonstrate their performance.

II. Stator Current Model under fault

The method used to study the influence of the load torque oscillation on the stator current is based on the magnetomotive force (MMF) and permeance wave approach. This approach is traditionally used for the calculation of the magnetic airgap field with respect to rotor and stator slotting or static and dynamic eccentricity [6] [7].

The detailed theoretical development for the stator current in case of load torque oscillation has been given in [8] to identify the consequence of bearing faults and in [9] for the general case. The results will be shortly resumed in the following.

As this paper considers variable speed drives, the supply frequency f_s and the fault frequency f_c can be considered variable. Note that f_c can be for example the time-varying rotational frequency f_r. The theoretical analysis of the stator current under fault, however, is identical to the steady state if relatively slow frequency variations are considered.

Under a mechanical fault, the load torque as a function of time is assumed to be described by a constant component Γ_{const} and an additional component varying at the fault characteristic frequency f_c. The first term of the variable component Fourier series is a cosine with frequency f_c. For the sake of clarity, higher order terms are neglected in the following and only the fundamental term is considered. The load torque can therefore be described by:

$$\Gamma_{load}(t) = \Gamma_{const} + \Gamma_c \cos(\omega_c t) \tag{1}$$

where Γ_c is the amplitude of the load torque oscillation and $\omega_c = 2\pi f_c$.

Considering the mechanical equation of the machine, the oscillating load torque leads to periodic oscillations at f_c of the mechanical rotor speed. The consequence is an oscillation at the same frequency on the mechanical rotor position. If the fundamental rotor MMF is calculated in the stator reference frame by using the transformation between the two reference frames, the oscillating mechanical rotor position produces an oscillating rotor MMF $F_r(\theta, t)$ that can be expressed as follows:

$$F_r(\theta, t) = F_r \cos(p\theta - \omega_s t - \beta' \cos(\omega_c t)) \tag{2}$$

with:

$$\beta' = p\frac{\Gamma_c}{J\omega_c^2} \tag{3}$$

where p is the pole pair number, J the total inertia and $\omega_s = 2\pi f_s$. The fault effect on the rotor MMF can be seen as a sinusoidal phase modulation at the characteristic fault frequency.

The stator MMF $F_s(\theta, t)$ is not directly affected and takes the same expression as in the healthy case:

$$F_s(\theta, t) = F_s \cos\left(p\theta - \omega_s t - \varphi_s\right) \tag{4}$$

where φ_s denotes the initial phase angle between rotor and stator MMF.

The total magnetic flux density is obtained by the multiplication of the total MMF with the airgap permeance, which is supposed constant. The induced voltage in a machine winding is related to the magnetic airgap field, so that the phase modulation is preserved. Consequently, a mechanical load fault leads to the following stator current expression (for an arbitrary machine phase):

$$\begin{aligned} i(t) &= i_{st}(t) + i_{rt}(t) \\ &= I_{st} \sin\left[\omega_s(t)t + \varphi_s\right] \\ &\quad + I_{rt} \sin\left[\omega_s(t)t + \beta \cos\left(\omega_c(t)t\right)\right] \end{aligned} \tag{5}$$

$i_{st}(t)$ and $i_{rt}(t)$ denote the stator current components resulting from the stator and rotor MMF. The amplitudes I_{st} and I_{rt} are supposed quasi-constant. β is the phase modulation index and it is proportional to Γ_c/ω_c^2. The healthy case is obtained considering $\beta = 0$.

For the sake of simplicity, the time harmonics of rotor MMF and the non-uniform airgap permeance have not been considered. However, the harmonics of supply frequency f_s and the rotor slot harmonics theoretically show the same phase modulation as the fundamental stator current component.

III. Time-Frequency Signal Processing

The time-varying supply frequencies in variable speed drives lead to non-stationary signals that require advanced signal processing methods for analysis. Traditional spectral estimation methods based on the Fast Fourier Transform (FFT) can no longer be applied. One possible solution for signal analysis is the use of time-frequency distributions [10] [11] that represent the signal energy with respect to time and frequency.

A multitude of possible time-frequency distributions exist with different properties. A simple method is the spectrogram that uses the FFT on a sliding window. It was applied in [12] to induction motor fault diagnosis. However, this method cannot provide a high resolution in time and frequency due to the Heisenberg-Gabor uncertainty principle [11]. The Wigner Distribution, proposed by Wigner in [13] and applied to signal processing by Ville [14], provides a high resolution in time and frequency. It is particularly adapted to the analysis of linearly varying frequencies, as can often be found in electrical drives.

A. Wigner Distribution

The Wigner Distribution (WD) is defined as follows:

$$W_x(t, f) = \int_{-\infty}^{+\infty} x\left(t + \frac{\tau}{2}\right) x^*\left(t - \frac{\tau}{2}\right) e^{-j2\pi f\tau} d\tau \tag{6}$$

This formula can be seen as the Fourier transform of a kernel $K_x(\tau, t)$ with respect to the delay variable τ. The kernel is similar to an autocorrelation function.

An interesting property of the WD is its perfect concentration on the instantaneous frequency in the case of a linear frequency modulation. However, other types of modulations (e.g. in our case sinusoidal phase modulations) produce so-called inner interference terms in the distribution [15]. Note

that the interferences may however be used for detection purposes as it will be shown in the following.

Another important drawback of the distribution is its non-linearity due to the quadratic nature. When the sum of two signals is considered, so-called outer interference terms appear in the distribution at time instants or frequencies where there should not be any signal energy [15]. If harmonic signals such as the stator current are analyzed, appropriate filtering is necessary. In order to avoid further interferences, the WD should be calculated using the analytical signal obtained through the Hilbert transform [11].

In practice, the Pseudo Wigner Distribution (PWD), a smoothed version of the WD, is often used. PWD is defined as follows [11]:

$$PW_x(t,f) = \int_{-\infty}^{+\infty} p(\tau) x\left(t+\frac{\tau}{2}\right) x^*\left(t-\frac{\tau}{2}\right) e^{-j2\pi f\tau} d\tau \tag{7}$$

where $p(\tau)$ is the smoothing window which also reduces the amplitudes of the interference terms.

B. Wigner Distribution of Stator Current in Steady State

In order to obtain the WD of the stator current according to (5) with constant supply and fault frequency, the WD of an analytical phase modulated signal $i_{rt}(t)$ will first be calculated with

$$i_{rt}(t) = I_{rt} \exp j\big[\omega_s t + \beta\cos(\omega_c t)\big] \tag{8}$$

The kernel of this signal can be written as follows :

$$\begin{aligned} K_{i_{rt}}(t,\tau) &= i_{rt}\left(t+\frac{\tau}{2}\right) i_{rt}^*\left(t-\frac{\tau}{2}\right) \\ &= I_{rt}^2 \exp j\left\{\omega_s\tau - 2\beta\sin(\omega_c t)\sin\left(\frac{\omega_c}{2}\tau\right)\right\} \end{aligned} \tag{9}$$

The WD is obtained as the Fourier transform (FT) of the kernel with respect to the delay τ:

$$\begin{aligned} W_{i_{rt}}(t,f) &= \mathrm{FT}_\tau\left\{K_{i_{rt}}(t,\tau)\right\} \\ &= I_{rt}^2\,\mathrm{FT}_\tau\Big\{\exp j\left(\omega_s\tau\right)\Big\} \\ &\quad * \mathrm{FT}_\tau\left\{\exp j\left[-2\beta\sin(\omega_c t)\sin\left(\frac{\omega_c}{2}\tau\right)\right]\right\} \end{aligned} \tag{10}$$

where $*$ denotes the convolution. The FT of the second term may be calculated in analogy to the FT of a pure PM signal using the Jacobi-Anger expansion [16] given by:

$$e^{j\gamma\sin\theta} = \sum_{n=-\infty}^{+\infty} J_n(\gamma) e^{jn\theta} \tag{11}$$

where J_n denotes the n-th order Bessel function of the first kind.

The second term in equation (10) can therefore be developed into a Fourier series which allows a simple calculation of its FT.

$$\begin{aligned} W_{i_{rt}}(t,f) &= I_{rt}^2\,\delta(f-f_s) \\ &\quad * \mathrm{FT}_\tau\left\{\sum_{n=-\infty}^{+\infty} J_n\big(-2\beta\sin(\omega_c t)\big) e^{jn\frac{\omega_c}{2}\tau}\right\} \\ &= I_{rt}^2 \sum_{n=-\infty}^{+\infty} J_n\big(-2\beta\sin(\omega_c t)\big)\,\delta\left(f-f_s-n\frac{f_c}{2}\right) \end{aligned} \tag{12}$$

where $\delta(f)$ is the Dirac delta function. For small modulation indexes β, the Bessel functions of order $n \geq 2$ are very small and may be neglected (narrowband approximation from communication theory):

$$\begin{aligned} W_{i_{rt}}(t,f) \approx\; & I_{rt}^2 J_0(\gamma)\,\delta(f-f_s) \\ & + I_{rt}^2 J_1(\gamma)\,\delta(f-f_s-\frac{f_c}{2}) \\ & - I_{rt}^2 J_1(\gamma)\,\delta(f-f_s+\frac{f_c}{2}) \end{aligned} \tag{13}$$

with $\gamma = -2\beta\sin(\omega_c t)$. The WD of the considered pure phase modulated signal is therefore a central frequency at f_s with sidebands at $f_s \pm f_c/2$. All the components have time-varying amplitudes at frequency f_c as γ is a function of time. It is important to notice that the lower sideband has the opposed sign to the upper sideband.

The Bessel functions $J_0(\gamma)$ and $J_1(\gamma)$ can be approximated for small arguments γ by [16]:

$$J_0(\gamma) \approx 1 \tag{14}$$

$$J_1(\gamma) \approx \frac{\gamma}{2} = -\beta\sin(\omega_c t) \tag{15}$$

As the stator current signal is considered as the sum of two components, a phase modulated signal and a pure frequency (see (5)), its WD must be calculated according to the following expression for the sum of two signals $x+y$ [11]:

$$W_{x+y}(t,f) = W_x(t,f) + W_y(t,f) + 2\,\mathrm{Re}\{W_{xy}(t,f)\} \tag{16}$$

with

$$W_{xy}(t,f) = \int_{-\infty}^{+\infty} x\left(t+\frac{\tau}{2}\right) y^*\left(t-\frac{\tau}{2}\right) e^{-j2\pi f\tau} d\tau \tag{17}$$

The WD of the pure frequency $i_{st}(t) = I_{st}\sin(\omega_s t + \varphi_s)$ (first term of (5)) is given by $I_{st}^2\,\delta(f-f_s)$. A detailed calculation of the cross terms $W_{i_{st}i_{rt}}$ shows that they are of small amplitude and that they do not introduce new frequency components. Thus, the cross terms may be neglected in this case and the following approximate expression is obtained for the WD of (5) :

$$\begin{aligned} W_{i_{st}+i_{rt}}(t,f) \approx\; & \left(I_{rt}^2 + I_{st}^2\right)\,\delta(f-f_s) \\ & - I_{rt}^2\beta\sin(\omega_c t)\;\delta(f-f_s-\frac{f_c}{2}) \\ & + I_{rt}^2\beta\sin(\omega_c t)\;\delta(f-f_s+\frac{f_c}{2}) \end{aligned} \tag{18}$$

In contrast to the pure phase modulated signal, the constant component I_{st} is present at the fundamental frequency. The fault characteristic signature is conserved.

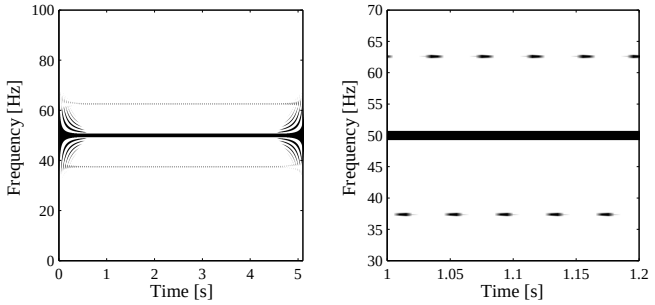

(a) Global view (b) Detail

Fig. 1. Pseudo Wigner Distribution of simulated steady state PM signal

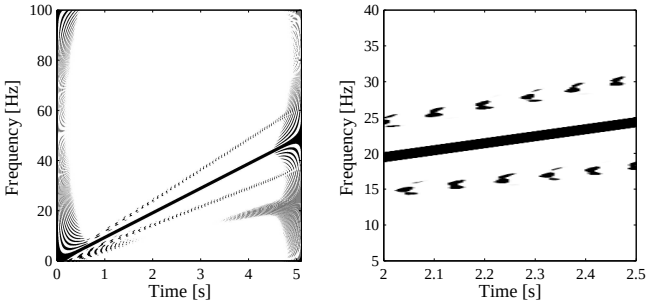

(a) Global view (b) Detail

Fig. 2. Pseudo Wigner Distribution of simulated transient PM signal

These considerations are illustrated in Fig. 1 where a detail of the PWD of the PM signal $s_1(t)$ is displayed. The plot is in logarithmic scale and only positive values are displayed. $s_1(t)$ is the sum of a pure sine and a sinusoidal PM signal:

$$s_1(t) = \cos\left(2\pi f_s t + \pi/8\right) + \cos\left(2\pi f_s t + \beta\cos\left(2\pi f_c t\right)\right) \tag{19}$$

with f_s=50 Hz, f_c=25 Hz, β=0.05 and sampling frequency 200 Hz. The PWD of $s_1(t)$ clearly shows the theoretically predicted signature: a strong component is visible at f_s with sidebands at $f_s \pm f_c/2$. The sideband amplitudes are time varying at modulation frequency f_c. Furthermore, the two sidebands have opposed amplitudes at a given time instant.

C. Wigner Distribution of Transient Stator Current

During speed transients, the supply and fault frequencies are time-varying. For the calculation of the WD of a transient stator current under fault, these frequencies are modelled as linear functions of time:

$$f_s(t) = \alpha_s + \beta_s t \tag{20}$$

$$f_c(t) = \alpha_c + \beta_c t \tag{21}$$

The instantaneous frequencies $f_i(t)$ of a sinusoidal signal with these frequency laws would be (see [11]):

$$f_{i,s}(t) = \alpha_s + 2\beta_s t \tag{22}$$

$$f_{i,c}(t) = \alpha_c + 2\beta_c t \tag{23}$$

Using similar approximations as in the precedent part, the WD of a transient current signal becomes:

$$\begin{aligned} W_i(t,f) \approx{}& \left(I_{rt}^2 + I_{st}^2\right)\,\delta\left(f - (\alpha_s + 2\beta_s t)\right) \\ &- I_{rt}^2\beta(t)\sin\left(\omega_c(t)t\right)\,\delta\left(f - (\alpha_s + 2\beta_s t) - \left(\frac{\alpha_c}{2} + \beta_c t\right)\right) \\ &+ I_{rt}^2\beta(t)\sin\left(\omega_c(t)t\right)\,\delta\left(f - (\alpha_s + 2\beta_s t) + \left(\frac{\alpha_c}{2} + \beta_c t\right)\right) \end{aligned} \tag{24}$$

The central component of the WD is now time-varying according to the instantaneous frequency law $f_{i,s}(t)$ of the fundamental stator current component. The sidebands are located at $f_{i,s}(t) \pm f_{i,c}(t)/2$ analogous to the stationary case. Their opposed amplitudes are also time-varying. It should also be noted that β is no longer constant during transients as it is proportional to $1/\omega_c^2$.

For illustration of the current signature in the transient case, consider Fig. 2 where the PWD of a transient signal is displayed. The signal is identical to $s_1(t)$ but with linearly varying supply and fault frequencies f_s and f_c in order to consider a case similar to a motor start-up. The modulation index β is kept constant in this example. The theoretically calculated signature is clearly visible. However, stronger interferences due to the time-varying frequencies can also be recognized.

IV. DSP Implementation

Two different detection algorithms based on stator current time-frequency analysis have been implemented on a DSP (see section IV-C). The DSP is a low-cost Analog Devices ADSP-21161 (21161N EZ-Kit lite), mainly designed for audio applications. The inputs include anti-aliasing filters, followed by 24-bit AD-converters with a minimum sampling rate of 48 kHz. As the fault signatures appear around the fundamental supply frequency of 50 Hz, a lower sampling rate would be advantageous but cannot be realized with this hardware. Therefore, a preprocessing stage with filtering and downsampling is implemented numerically before the calculation of the WD.

A. Preprocessing

1) Downsampling: The stator current is sampled at 48 kHz. However, relevant fault frequencies with the two pole pair machine are at a maximum frequency of 1.5 times the supply frequency f_s which leads approximately to 75 Hz for the considered machine in nominal conditions. As a consequence, a real-time downsampling stage is implemented to decrease the sampling frequency by a factor $2^8 = 256$ i.e. the new sampling frequency is 187.5 Hz. The implementation of a single lowpass filter with normalized cut-off frequency $1/(2 \cdot 256)$ followed by a 256-fold decimator (takes one sample out of 256) would require a high filter order and a significant amount of memory for storage. It is more efficient to implement a scheme as in figure 3 with 8 decimation stages in cascade, each including the same filter $H(f)$ with a normalized cut-off frequency 0.25 followed by a 2-fold decimator. Main benefits are a low global order, small time delay and computational cost.

More precisely, the implemented lowpass filter $H(f)$ is an elliptic IIR filter of order 14. Its normalized cut-off frequency at -3 dB is 0.227 so that after the last downsampling stage,

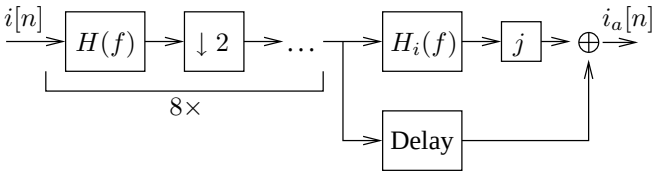

Fig. 3. Preprocessing of stator current signal: lowpass filter $H(f)$, decimation and Hilbert filter $H_i(f)$

frequencies between 0 and 85.03 Hz can be analyzed without significant attenuation.

2) Hilbert filtering: The Wigner Distribution should be calculated on the complex, analytical current signal in order to avoid interferences [11]. The analytical current signal $i_a[n]$ is obtained from the real current signal $i[n]$ by means of the Hilbert transform $H\{.\}$ according to:

$$i_a[n] = i[n] + jH\{i[n]\} \tag{25}$$

The Hilbert transform is realized using a Hilbert filter with the following frequency response:

$$H_i(f) = \begin{cases} -j & \text{for } 0 \le f \le \frac{1}{2} \\ j & \text{for } -\frac{1}{2} \le f < 0 \end{cases} \tag{26}$$

Its impulse response $h_i[n]$ is:

$$h_i[n] = \frac{2\sin^2(\pi n/2)}{\pi n} = \begin{cases} 0 & \text{if } n \text{ is even} \\ \frac{2}{\pi n} & \text{if } n \text{ is odd} \end{cases} \tag{27}$$

In practice, the Hilbert filter is implemented as finite impulse response filter of order N_i=257. In order to respect causality, the symmetric impulse response must be shifted by $(N_i-1)/2$. The filter output is therefore delayed by 128 samples corresponding to 0.688 s. The analytical signal $i_a[n]$ is obtained by multiplication of the filter output with j and addition of the delayed real signal $i[n]$ (see Fig. 3).

B. Discrete Implementation of the WD

The discrete Wigner Distribution (DWD) $W_x[n,k]$ of a discrete signal $x[n]$ of length N can be calculated according to the following formula [11] (verifier!):

$$W_x[n,m] = \frac{1}{N}\sum_{k=0}^{N-1} p[k]x[n+k]x^*[n-k]e^{-j4\pi mk/N} \tag{28}$$

where $p[k]$ is a window function. This expression can be efficiently implemented using an FFT algorithm (see [17] for a sample algorithm). In this work, the DWD is calculated on data records of length $N = 512$. The window function is a xx point Hamming (??) window.

The result of the calculation would be a (512×512) matrix that would require a considerable amount of memory for storage. However, the DWD can be calculated for each time bin n independently and the fault indicator can be directly derived for this time bin. This offers the advantage that no storage of the complete DWD is necessary, only the fault indicator is retained.

C. Fault Indicators

Two fault indicators based on the Wigner Distribution, called WD1 and WD2 in the following, are proposed. For comparison with traditional techniques, the results obtained with a spectrum based indicator are also presented in steady-state operation. All the fault indicators are calculated on data records of length 512 samples after downsampling. As soon as one data buffer of length 512 is complete, the fault indicator is calculated while the arriving samples are written to a second buffer. The calculation of the indicator must therefore take less than 2.73 s which is respected in all the cases.

1) Spectrum based indicator: The magnitude of the Fourier transform of the phase modulated stator current according to (5) is approximately for small β [9]:

$$|I(f)| \approx (I_{st} + I_{rt})\ \delta(f-f_s) + I_{rt}\frac{\beta}{2}\,\delta\left(f-(f_s \pm f_r)\right) \tag{29}$$

where the fault frequency is supposed to be f_r.

The algorithm that calculates the spectrum based fault indicator on a given buffer is the following:

- Zero-padding of initial data record up to 1024 samples
- Discrete Fourier transform using a Hanning window
- Search of the maximum absolute value of the Fourier transform I_m, corresponding to the supply frequency f_s
- Search of maxima I_1 and I_2 in intervals $[f_s - f_s/p, f_s - 0.9f_s/p]$ and $[f_s + 0.9f_s/p, f_s + f_s/p]$. The rotational frequency f_r is supposed to vary within these bounds under different load conditions.
- The spectrum based indicator is then given by $(I_1 + I_2)/I_m$

The normalization with respect to the fundamental amplitude I_m is useful to obtain an indicator value that depends less on the machine load level than without normalization.

2) Indicator WD1: The first indicator WD1 analyzes the energy in a region around the characteristic fault signature at $f_s \pm f_r/2$ in the PWD. The rotational frequency is supposed to vary between $0.9f_s/p$ and f_s/p as before. The fault indicator is only calculated for time bins varying from n=64 to 448 in order to avoid border regions with strong interferences. The detailed steps are the following:

- for n=64 to 448
  - Calculate DWD$[n,m]$
  - Determine frequency bin m_A belonging to strongest absolute value A (supply frequency)
  - Calculate frequency bins corresponding to intervals $I_1 = [(1 + 0.9/4)m_A, (1 + 1/4)m_A]$ and $I_2 = [(1 - 1/4)m_A, (1 - 0.9/4)m_A]$
  - A_1 and A_2 are the sums of the absolute value of DWD$[n,m]$ in the intervals I_1 and I_2
  - Normalization: WD1$[n] = (A_1 + A_2)/A$
- The fault indicator WD1 is the sum of all the WD1$[n]$

The normalization of the energy with respect to the fundamental is done for each time bin. As with the spectrum based indicator, it improves the indicator behavior under varying load levels. Since the fault signature is oscillating with positive and negative values in the PWD, the absolute values are taken.

For the second indicator WD2, two pseudo signals $s_u[n]$ and $s_l[n]$ are synthesized by recording at each instant the highest absolute value of the PWD in intervals I_1 and I_2. They represent the oscillating fault signature in the upper and lower sideband. According to (18), these signals theoretically oscillate at the fault frequency f_r and their amplitude is proportional to β. Once recorded, the spectrum of $s_1(n)$ and $s_2(n)$ is analyzed in an interval that takes into account possible values of f_r. This interval is calculated as a function of the minimum and maximum estimated supply frequency for the considered data record.

- for n=64 to 448
  - Calculate DWD$[n, m]$
  - Determine fundamental amplitude A and the intervals I_1 and I_2 as with WD1
  - Find maximum absolute value of DWD$[n, m]$ in I_1 and I_2 and retain the corresponding signed values A_u and A_l
  - Synthesis of the pseudo-signals including a normalization: $s_u[n] = A_u/A$, $s_l[n] = A_l/A$
- Calculate the minimum and maximum possible value of f_r based on the minimum and maximum supply frequency
- Discrete Fourier transform of s_u and s_l using 512 points (zero-padding) and a Hanning window
- Derivation of energies E_u and E_l in the interval $[f_{r,\min}, f_{r,\max}]$
- WD2 is the sum of E_u and E_l

This second indicator is more complex to calculate but it should be more accurate than WD1. Since WD1 takes the absolute values of the PWD in a time-frequency region, it can be influenced by noise or oscillating signatures at other frequencies. The indicator WD2 is only depending on the oscillating energy at certain frequencies which makes it insensitive to such phenomena.

V. Experimental Results

A. Description of Experimental Setup

Tests have been conducted on an experimental setup with a three phase, 400 V, 50 Hz, 5.5 kW Leroy Somer induction machine (see Fig. 4). The motor has two pole pairs and its nominal torque is about 36 Nm. The machine is supplied by a standard industrial inverter operating in open-loop condition with a constant voltage to frequency ratio. The load is a DC motor with separate, constant excitation connected to a resistor through a DC/DC converter. Measured quantities for off-line analysis are the 3 terminal voltages, 3 line currents, speed and load torque. All the signals are acquired at 25 kHz by a 24 bit data acquisition system. Further signal processing is done on a standard desktop PC using Matlab. In parallel, one line current signal is fed into the DSP for on-line analysis.

The load torque oscillations are produced as follows: a DC/DC converter (Buck) is used to control the DC motor armature current. Thus, a constant load torque with a small additional oscillating component can be introduced. The reference signal for the oscillation is generated by the DSP that receives position information from an incremental encoder.

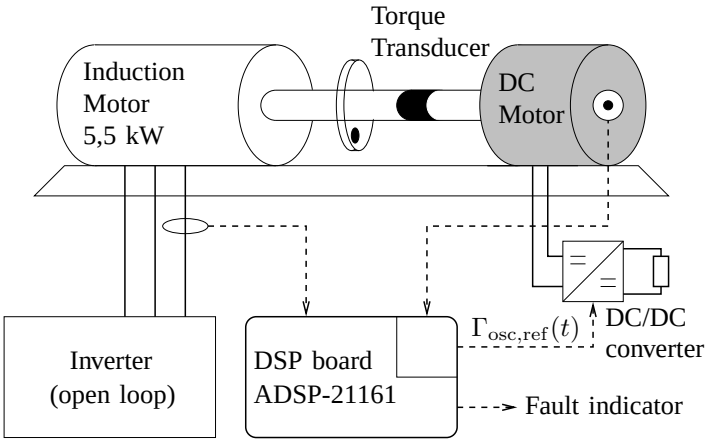

Fig. 4. Scheme of experimental setup

Therefore, the oscillating torque component Γ_{osc} is controlled with respect to the mechanical rotor position θ_r and takes the following form:

$$\Gamma_{osc}(t) = \Gamma_c \cos\left(\theta_r(t) + \varphi_r\right) \tag{30}$$

(Mentionner influence de phi !) Neither the position signal, nor a speed measurement is used for the stator current analysis in the DSP.

A load unbalance can be created by fixing a mass eccentrically on a disc placed on the shaft. In the following test, a mass of m=77 g has been fixed at a distance of r=75 mm from the center. The mass has two effects: first, the weight leads to a load torque oscillation of amplitude $\Gamma_c = mgr$ and it is varying sinusoidally with respect to the rotor position. Secondly, a centrifugal force acts on the shaft. An increasing level of dynamic eccentricity may result depending on the bearing tolerances and the stiffness of the shaft.

B. Steady-State Results

1) Off-line Analysis: The stator current has been recorded and processed off-line in order to study the fault effects on the stator current spectrum and the Wigner Distribution. The current spectrum shows a rise at frequencies $f_s \pm f_r$ with respect to the fault level as expected. Fig. 5 shows a detail of the WD of the healthy and faulty motor stator current at 50% load. The load torque oscillation amplitude in the faulty case was Γ_c=0.22 Nm. The theoretically calculated interference signature is present on the WD of the faulty current signal at $f_s \pm f_r/2 \approx 50 \pm 12.5$ Hz , whereas the WD of the healthy stator current does not show any energy at the considered frequencies. However, other interferences are present at frequencies close to the fundamental.

2) On-Line Analysis: The load torque oscillations in steady state are imposed according to the fault profile displayed in Fig. 6. During 20 data records (corresponding to 55 s), the DC machine armature current reference contains no oscillating component. Then, the amplitude of the oscillating component increases after each 20 data records in order to obtain 6 fault levels from Γ_c=0.03 to 0.22 Nm (measured values). Note that for the lowest fault level, Γ_c is only about 0.1% of the nominal motor torque.

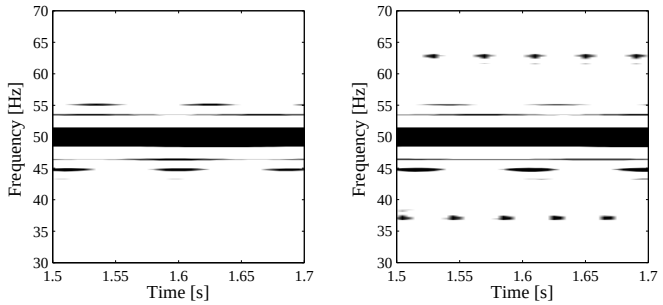

(a) healthy (b) faulty

Fig. 5. Pseudo Wigner Distribution of healthy and faulty stator current in steady state at 50% load

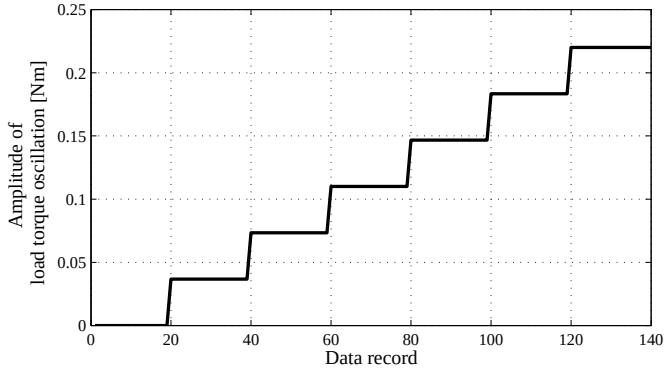

Fig. 6. Considered fault profile: Load torque oscillation amplitude Γ_c vs. data records

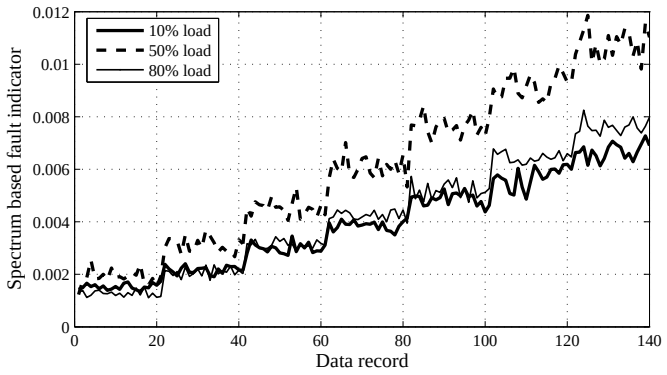

Fig. 7. Spectrum based fault indicator vs. data records

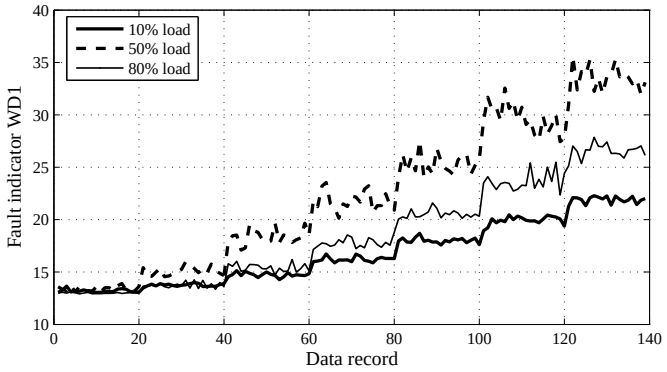

Fig. 8. Fault indicator WD1 vs. data records

The results obtained with the spectrum based fault indicator are shown in Fig. 7 for the nominal supply frequency and three different load levels. The indicator evolves approximately linearly with respect to the amplitude of the load torque oscillation. This is the case for all average load levels. Even the smallest torque oscillation of only 0.1% of the nominal torque can still be detected. However, the evolution of the indicator is sensitive to the average load level. The indicator is higher with 50% load than with small load or 80% load. This can be explained by the normalization with respect to the fundamental stator current amplitude, which is $I_{st} + I_{rt}$. But the sideband amplitudes are βI_{rt}, i.e. the correct normalization should only use the rotor current amplitude I_{rt} which is unfortunately not directly available. Nevertheless, it can be observed that the proposed normalization improves the dependence of the indicator on the load level compared to no normalization at all.

The results obtained under the same test conditions with the two indicators based on the Wigner Distribution, WD1 and WD2 are displayed in Figs. 8 and 9. Both indicators show an approximately linear rise with respect to the amplitude of the load torque oscillation. The indicator WD2 seems more sensitive to the increase of Γ_c than WD1. A possible explanation is the more precise analysis with respect to the fault frequency in case of WD2. WD1 is based on the total energy in the WD in a given frequency interval, whereas WD2 only considers the energy of pulsating components at fault frequency. It can also be noticed that WD2 depends less on the average load level than WD1.

Additional tests at lower supply frequency were conducted to verify the fault indicator behavior at lower speed. The fault indicators are quantities that should represent the evolution of the PM modulation index β. β is proportional to $1/\omega_c^2$ according to the theoretical development and the fault indicator should therefore show the same behavior. This was verified with a supply frequency f_s=25 Hz which leads approximately to half the fault frequency f_c. The indicator should therefore be four times higher compared to f_s=50 Hz. Fig. 10 shows the spectrum based fault indicator and WD1 for the two different supply frequencies. The healthy state of all the indicators was referenced to zero. The indicators at f_s=50 Hz were multiplied

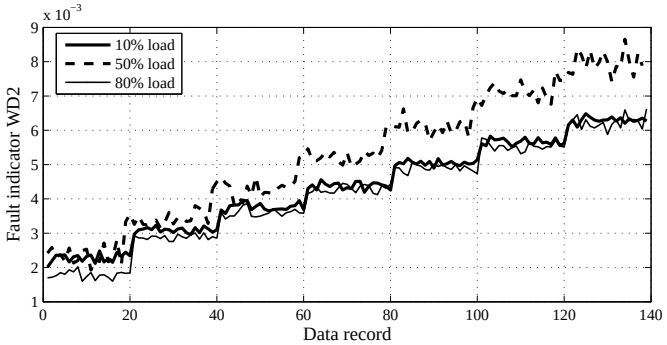

Fig. 9. Fault indicator WD2 vs. data records

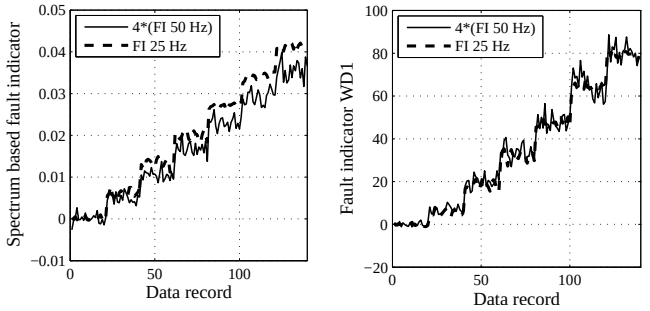

(a) Spectrum based fault indicator (b) Fault indicator WD1

Fig. 10. Fault indicators at 25 Hz and 50 Hz supply frequency vs. data records

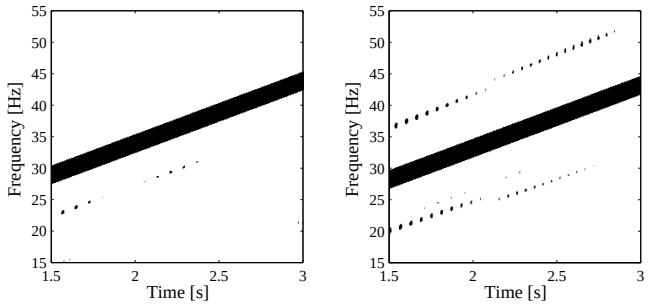

(a) healthy (b) faulty

Fig. 12. Pseudo Wigner Distribution of healthy and faulty stator current during speed transient at 50% load

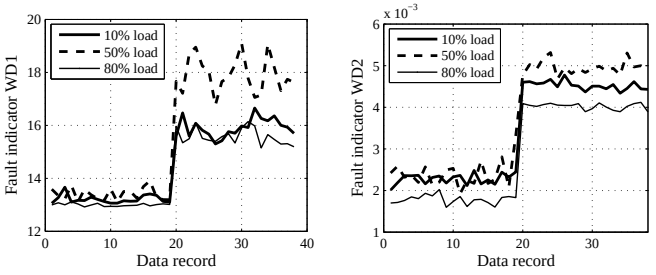

(a) Fault indicator WD1 (b) Fault indicator WD2

Fig. 11. Fault indicators WD1 and WD2 in healthy state (data records 1 to 19) and with load unbalance (data records 20 to 40)

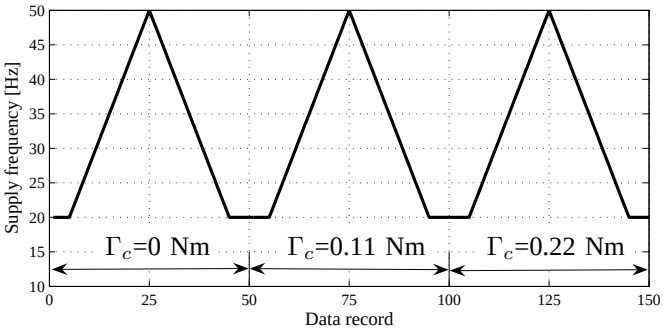

Fig. 13. Considered speed profile: Supply frequency f_s vs. data records and corresponding torque oscillation amplitude

by four to allow the comparison. A good agreement between the indicators can be found, especially for WD1, which proves experimentally that $\beta \propto 1/\omega_c^2$. The results with the indicator WD2 are not displayed, but they are similar to those obtained with the spectrum based indicator.

3) Load unbalance: The three proposed fault detection schemes are tested with an unbalanced load. Th small mass leads theoretically to a sinusoidal torque oscillation of amplitude 0.057 Nm. The results obtained with the WD based fault indicators at f_s=50 Hz are displayed in Fig. 11. Both indicators clearly detect the fault under all tested load conditions. The magnitude of the indicators in the faulty case is comparable to the second or third fault level in the precedent tests, corresponding to values of Γ_c from 0.07 to 0.11 Nm. The values are higher than expected, possibly due to effects of the centrifugal force. As in case of the load torque oscillations, WD2 is less dependent on the load level than WD1. Despite of the indicator dependence on the load level, a simple detector using the same threshold for all load levels could be employed.

C. Results during Transient Operation

1) Off-line Analysis: The stator current has been recorded during a motor start-up from 0 to 50 Hz supply frequency in 5 s. The WDs of the healthy and faulty stator current can be compared in Fig. 12 for 50% average load and Γ_c=0.22 Nm. The expected interference signature is visible at $f_s \pm f_r/2$ in the faulty case.

2) On-line Analysis: The algorithms used in the preceding section for steady-state current analysis are tested under motor operation at variable speed. One modification of the described algorithms is necessary for a correct functioning: Until now, the algorithms have estimated a quantity directly proportional to the phase modulation index β in (5). However, β depends on the fault characteristic frequency f_c that itself depends on f_r and f_s (see (3)). Therefore, the obtained fault indicator with the precedent algorithms must be multiplied by f_c^2 to yield a result independent of speed. Since f_c and f_r are directly proportional to f_s, it is equivalent to multiply the indicator with the estimated value of f_s.

The speed profile used in the following tests is displayed in Fig. 13. During one speed cycle, the supply frequency f_s varies linearly from 20 Hz to 50 Hz during 20 data records and back to 20 Hz in the same way. At the start and at the end of one cycle, f_s is constant during 5 data records. This speed cycle is repeated three times: first without a load torque oscillation, then with Γ_c=0.11 Nm and Γ_c=0.22 Nm. The lowest supply frequency is 20 Hz because of the DC machine voltage drop. Below this value, the DC motor armature current control is no more possible and therefore, the torque oscillation are not correctly produced.

The tests with the first fault indicator WD1 gave the results displayed in Fig. 14 for two constant average load torques corresponding to 10% and 70% load. During the first speed cycle without any oscillating torque, the indicator shows variations and is therefore still speed dependent with higher values at higher motor speed. When the first level of torque oscillation is applied from data record 50 on, the indicator jumps to a higher value. During the second speed cycle, the indicator value still depends on the speed but the relative variations

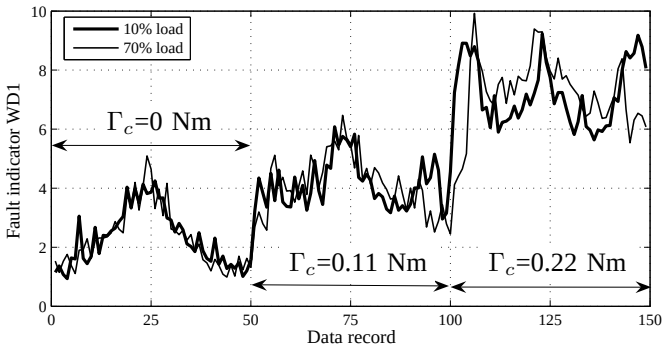

Fig. 14. Fault indicator WD1 vs. data records during speed transients

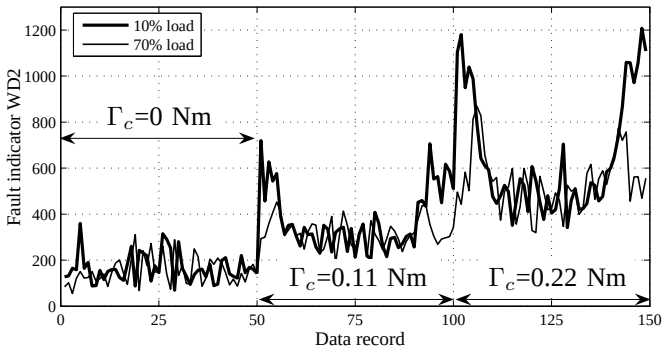

Fig. 15. Fault indicator WD2 vs. data records during speed transients

between f_s=20 Hz and f_s=50 Hz are much smaller. The same behavior can be observed during the third speed cycle with a higher oscillating torque. It can be concluded from these tests that the fault indicator WD1 still depends on the speed, despite of the previously mentioned indicator correction. A simple threshold cannot clearly distinguish between the healthy case and Γ_c=0.11 Nm (0.3% of nominal torque). However, for a given speed or supply frequency, the fault indicator is always higher with the torque oscillation. With stronger oscillations (Γ_c=0.22 Nm or 0.6% of nominal torque), the discrimination is possible for all considered speeds.

The results obtained with the second indicator WD2 are shown in Fig. 15 for the same two load levels. It can be noted that is less varying during the first speed cycle compared to WD1. The behavior during the following cycles with torque oscillation shows higher indicator values at low speed whereas the indicator is approximately constant above a certain minimal supply frequency (about 30 Hz).

VI. Conclusion

This paper studied the detection of mechanical faults in induction motor drives at variable speed using stator current time-frequency analysis with the Wigner Distribution. The fault related torque oscillations modulate the phase of the stator current signal and lead to a characteristic signature on the Wigner Distribution. Fault indicators can be calculated using properties of this interference structure. The two proposed methods and a classical spectrum based indicator have been implemented on a DSP for on-line condition monitoring. Tests in steady-state have shown that load unbalance and small torque oscillations can be detected.

Acknowledgment

The authors would like to thank...

References

[1] W. T. Thomson, “On-line current monitoring to detect electrical and mechanical faults in three-phase induction motor drives,” in *Proc. International Conference on Life Management of Power Plants*, Dec. 1994, pp. 66–73.

[2] R. R. Obaid, T. G. Habetler, and D. J. Gritter, “A simplified technique for detecting mechanical faults using stator current in small induction motors,” in *Proc. IEEE Industry Applications Society Annual Meeting, 2000*, Rome, Italy, Oct. 2000, pp. 479–483.

[3] C. Kral, T. G. Habetler, and R. G. Harley, “Detection of mechanical imbalances of induction machines without spectral analysis of time-domain signals,” *IEEE Trans. Ind. Applicat.*, vol. 40, no. 4, pp. 1101–1106, July/Aug. 2004.

[4] M. Blödt, M. Chabert, J. Regnier, J. Faucher, and B. Dagues, “Detection of mechanical load faults in induction motors at variable speed using stator current time-frequency analysis,” in *Proc. IEEE International Symposium on Diagnostics for Electric Machines, Power Electronics and Drives (SDEMPED ’05)*, Vienna, Austria, Sept. 2005.

[5] S. Rajagopalan, J. A. Restrepo, J. M. Aller, T. G. Habetler, and R. G. Harley, “Wigner-Ville distributions for detection of rotor faults in brushless DC (BLDC) motors operating under non-stationary conditions,” in *Proc. IEEE International Symposium on Diagnostics for Electric Machines, Power Electronics and Drives (SDEMPED ’05)*, Vienna, Austria, Sept. 2005.

[6] J. R. Cameron and W. T. Thomson, “Vibration and current monitoring for detecting airgap eccentricities in large induction motors,” *IEE Proceedings*, vol. 133, no. 3, pp. 155–163, May 1986.

[7] B. Heller and V. Hamata, *Harmonic Field Effects in Induction Machines*. Amsterdam, Netherlands: Elsevier, 1977.

[8] M. Blödt, P. Granjon, B. Raison, and G. Rostaing, “Models for bearing damage detection in induction motors using stator current monitoring,” in *Proc. IEEE International Symposium on Industrial Electronics (ISIE ’04)*, Ajaccio, France, May 2004, pp. 383–388.

[9] M. Blödt, M. Chabert, J. Faucher, and B. Dagues, “Mechanical load fault detection in induction motors by stator current time-frequency analysis,” in *Proc. IEEE International Electric Machines and Drives Conference (IEMDC ’05)*, San Antonio, Texas, May 2005.

[10] B. Boashash, *Time Frequency Signal Analysis and Processing - A Comprehensive Reference*, 1st ed. Oxford, UK: Elsevier, 2003.

[11] P. Flandrin, *Time-Frequency/Time-Scale Analysis*. San Diego: Academic Press, 1999.

[12] K. Bacha, M. Gossa, H. Henao, and G. A. Capolino, “A time-frequency method for multiple fault detection in three-phase induction machines,” in *Proc. IEEE International Symposium on Diagnostics for Electric Machines, Power Electronics and Drives (SDEMPED ’05)*, Vienna, Austria, Sept. 2005.

[13] E. Wigner, “On the quantum correction for thermodynamic equilibrium,” *Physical Review*, vol. 40, no. 5, pp. 749–759, June 1932.

[14] J. Ville, “Théorie et applications de la notion de signal analytique,” *Câbles et Transmissions*, vol. 2, no. 1, pp. 61–74, 1948.

[15] W. Mecklenbräuker and F. Hlawatsch, Eds., *The Wigner Distribution — Theory and Applications in Signal Processing*. Amsterdam (The Netherlands): Elsevier, 1997.

[16] M. Abramowitz and I. A. Stegun, *Handbook of Mathematical Functions with Formulas, Graphs, and Mathematical Tables*, nineth ed. New York: Dover Publications, 1964.

[17] F. Auger, P. Flandrin, P. Gonalvs, and O. Lemoine. (1995/1996) Time-frequency toolbox. CNRS / Rice University. France. [Online]. Available: http://crttsn.univ-nantes.fr/∼auger/tftb.html